scientific reports

OPEN

Layered double hydroxides in nanofiltration as a new approach to nitrate removal

Hossein Haji Mohammadi Shire Jini[1], Zahra Zangeneh[1], Toraj Mohammadi[1✉] & Abbas Akbarzadeh[2]

High nitrate concentrations in water present serious risks to human health. This study evaluates two removal strategies: layered double hydroxide (LDH) nanoparticles (NPs) and LDH-incorporated thin-film composite nanofiltration (TFC-NF) membranes to reduce nitrate concentration. First, Mg–Al, Ni–Fe, and Mn-impregnated Zn–Al LDH NPs were co-precipitated, characterized using X-ray diffraction (XRD), Fourier-transform infrared spectroscopy (FTIR), Brunauer-Emmett-Teller (BET) analysis, field emission scanning electron microscopy (FESEM), and zeta potential measurement, and tested in batch adsorption experiments (20 mg/L nitrate solution, 1 g/L adsorbent dosage). Among the LDH NPs tested, Ni–Fe LDH demonstrated the highest nitrate rejection, achieving 13–14% at this concentration, with no significant change with further calcination. Next, the TFC-NF membranes were fabricated by embedding LDH NPs into the support layer; one variant received additional layer-by-layer (LBL) surface modification. The membranes were also characterized using FESEM and then evaluated using a 50 mg/L nitrate solution at 6 bar pressure and 25 °C. The TFC-NF membrane containing 0.25 wt% Mn-impregnated Zn–Al LDH achieved nitrate rejection of 43% with pure water flux (PWF) of 4.5 L/m^2 h bar^{-1}. Under the same conditions, the LBL-TFC NF membrane showed lower nitrate rejection of 17% but higher PWF of 7.7 L/m^2 h bar^{-1}.

Keywords Nitrate removal, Nanofiltration (NF) membrane, Layered double hydroxide (LDH), Thin film composite (TFC), Layer-by-layer (LBL) assembly

Intensified agricultural activity, rapid urbanization, and industrial expansion have dramatically increased nitrate inputs to both groundwater and surface water worldwide. Excessive application of synthetic and organic fertilizers, coupled with inadequate sewage treatment and improper disposal of human and animal waste, have also accelerated soil nitrification and leaching processes, pushing nitrate concentrations well above natural background levels[1–3].

Land-use changes over the past century, particularly the transition from natural ecosystems to cropland and densely populated urban areas, have fundamentally altered the nitrogen cycle, increasing the rates at which nitrogen is mineralized, mobilized, and transported to aquatic systems[4]. Long-term exposure to high NO_3^- levels in water can cause methemoglobinemia in babies, and also carcinogenic nitrosamines[5,6], thyroid[7], and cancer[8] are the main impacts of its high concentration in drinking water. Identifying and analyzing NO_3^- pollution is critical for watershed pollution control planning. Potential sources of NO_3^- in water bodies include synthetic and organic fertilizers, manure, sewage, soil nitrogen, and air deposition[9]. The World Health Organization (WHO) limits pollutant nitrate levels to 50 mg/L in drinking water[10,11].

Nitrate (NO_2^-) is highly soluble and chemically stable, meaning it does not readily precipitate or adsorb onto soil particles under typical environmental conditions. As a result, once introduced, it is difficult to remove using conventional water-treatment methods such as coagulation, sedimentation, or standard filtration[12]. Several approaches have been studied for the removal of nitrate from water and wastewater, such as biological denitrification[13], chemical reduction[14], membrane separation[15], capacitive deionization[16], and adsorption[17,18]. Although some of these approaches can yield positive results, they frequently encounter drawbacks such as substantial operational expenses, energy demands, and generation of waste brine[19].

Membrane technology could be efficient for preventing secondary contamination in treated water from chemical compounds and microorganisms. Nanofiltration (NF) and reverse osmosis (RO) membrane processes

[1]Center of Excellence for Membrane Research and Technology, Department of Chemical, Petroleum and Gas Engineering, Iran University of Science and Technology (IUST), Narmak, Tehran, Iran. [2]Water Research Institute, Tehran, Iran. ✉email: torajmohammadi@iust.ac.ir

are promising methods for treating groundwaters with high nitrate levels due to their efficiency, ease of operation, high effluent water quality, modularity, and flexibility. These technologies require water to cross a membrane under pressure to reject ionic species such as nitrate in the waste stream[10,17]. RO removes all ions, makes water purified. Therefore, desalinated water pH fluctuates until managed[4].

NF operates on hydrostatic pressure to carry molecules across semipermeable membranes, such as ultrafiltration (UF) and RO. Larger molecules are restricted by the membranes, whereas low-molecular-weight solutes and solvents pass through. Recently, NF has been more widely employed in water, food, pharmaceuticals, chemical, and wastewater treatment[20,21]. The main difference between NF and UF is the membrane's pore size and charge and component molecular weight. The molecular weight threshold for NF membranes is 400–500 Da, with pore sizes of 0.5–2 nm[22,23]. Also requires 3–20 bar operating pressure[24]. NF systems are more flux-efficient than RO and can purify water in many industries and applications[25].

El-Ghzizel et al. applied a 12 m^3/day NF (NF90) pilot plant to reduce nitrate concentration from 68 to 18 mg NO_3^-/L with 75% recovery rate. The above results were obtained with 5 bar feed pressure and 0.2 kWh/m^3 energy consumption[10]. Hayrynen et al.[26] reduced nitrate content from mine water employing NF, Filmtec Corp. thin-film composite (TFC) membranes. The nitrate concentration in water was 69 mg/L, however, the NF membrane treatment decreased it to 51 mg/L with 25% rejection rate. Mahvi et al. investigated that initial nitrate, co-existing anions, and TDS affect the NF nitrate elimination. The results showed that increasing initial nitrate concentration in the solution lowers NF membrane nitrate removal performance. The clearance rate dropped from 80.5% at 100 mg/L to 70.3% at 300 mg/L nitrate. Co-ions in the solution also slows down nitrate elimination. When the interfering ions manipulate from 50 to 250 mg/L, nitrate removal efficiency drops from 65.1 to 25.2% in Na_2SO_4 and from 74.1 to 59.5% in NaCl solutions[27].

LDH nanoparticles (NPs) have been widely used for nitrate removal. The molecular structure of LDHs with the general chemical formula is $[M^{(II)}_{1-x}M^{(III)}_x(OH)_2]^{x+}[A^{n-}_{x/n} \cdot yH_2O]^{x-}$, where $M^{(II)}$ represents divalent metals (Mg^{2+} Ca^{2+}, Mn^{2+}, Zn^{2+}, Fe^{2+}, etc.) and $M^{(III)}$ represents trivalent metals (Mn^{3+}, Al^{3+}, Fe^{3+}, etc.), where cations are placed in an octahedral unit. In the general formula, x represents the ratio of $\frac{M^{(II)}}{M^{(II)}+M^{(III)}}$, while y is the number of water molecules between the layers. Also, A^{n-} is an interlayer anion, and the most common of which is Cl^-, CO_3^{2-}, NO_3^- or ClO_4^-, which represents a hydrated interlayer anion with n valency to neutralize the positive charge of LDH and holds the layers of the LDH structure together by the weak interlayer forces[28,29]. Due to their multidimensional character, LDHs may be employed as two-dimensional (2D) NPs for the deliberate creation of polymer nanocomposites. LDHs may be synthesized using many ways; however, the co-precipitation technique is commonly employed because of its simplicity[30,31]. The structure of LDHs comes from brucite ($Mg(OH)_6$), where the replacement of trivalent ions with divalent ions results in a positive charge that is neutralized by interlayer anions. Consequently, LDHs have remarkable anion-exchange capabilities[32]. Nevertheless, LDHs have several limitations, including the potential for aggregation, which decreases their adsorption efficacy by blocking adsorption sites; hence, selecting an appropriate carrier is essential[33]. Zhuwu Jiang et al. reported a removal percentage of 85.3% using Mg-Al LDH solution with an initial nitrate concentration of 5 mg/L[34].

In this article, LDH NPs were synthesized and their nitrate removal capabilities were evaluated. An attempt was made to improve their nitrate adsorption capacities. As said, because they have adsorption characteristics, they may have some disadvantages with NF membranes, which face problems despite their good performance. Also, they were embedded in NF membranes via layer-by-layer (LBL) assembly and their performance was investigated in nitrate removal and desalination experiments.

Materials and methods
Materials
For membrane fabrication, *N*-Methyl-2-pyrrolidone (NMP) and normal heptane (n-heptane) were purchased from Merck. Polyvinylpyrrolidone K30 (PVP), Polysulfone (PSF), Trimesoyl chloride (TMC), Piperazine (PIP), Poly(diallyldimethylammonium chloride) (PDDA), Poly(sodium 4-styrene sulfonate) (PSS), and Glutaraldehyde (GA) were purchased from Sigma-Aldrich. For NPs synthesis, Nickel chloride ($NiCl_3$), Iron chloride ($FeCl_3$), Sodium carbonate (Na_2CO_3), Sodium chloride (NaCl), Magnesium chloride ($MgCl_2$), Aluminum chloride ($AlCl_3$), Manganese(II) chloride tetrahydrate ($MnCl_2.4H_2O$), and Zinc chloride hexahydrate ($ZnCl_2 \cdot 6H_2O$) were purchased from Sigma-Aldrich. Purolite A-400 ion exchange resin was purchased from PUROLITE CO. Also, HCl and NaOH were purchased from Sigma-Aldrich for pH adjustment. Potassium nitrate (KNO_3), was selected for nitrate rejection, and Na_2SO_4, $MgSO_4$, and $MgCl_2$, were selected for desalination tests, were purchased from Sigma-Aldrich. Deionized (DI) water was used to prepare solutions.

LDH synthesis
LDH NPs were synthesized via the co-precipitation method as described by Andrés Cano et al.[35] and presented in Fig. 1.

Mg–Al LDH
In the synthesis of this type of NPs, the molar ratio of magnesium to aluminum was considered 4:1[36]. For this purpose, 25.41 g of $MgCl_2 \cdot 6H_2O$ was weighed and dissolved with 16.66 g of $AlCl_3$ in 200 mL of distilled water. Then, 1 M solution of sodium hydroxide was prepared. It was used to adjust the final solution pH to 10. Finally, 21.20 g of sodium carbonate was added to 200 mL of distilled water (1 M). At this step, the metal, alkali, and carbonate solutions were added drop by drop to distilled water at 60 °C, and the solution was placed on a mechanical stirrer for 24 h. Then, the obtained solution was washed with distilled water until its pH becomes neutral. In the last step, the NPs were placed inside the oven at 80 °C to dry and then ground.
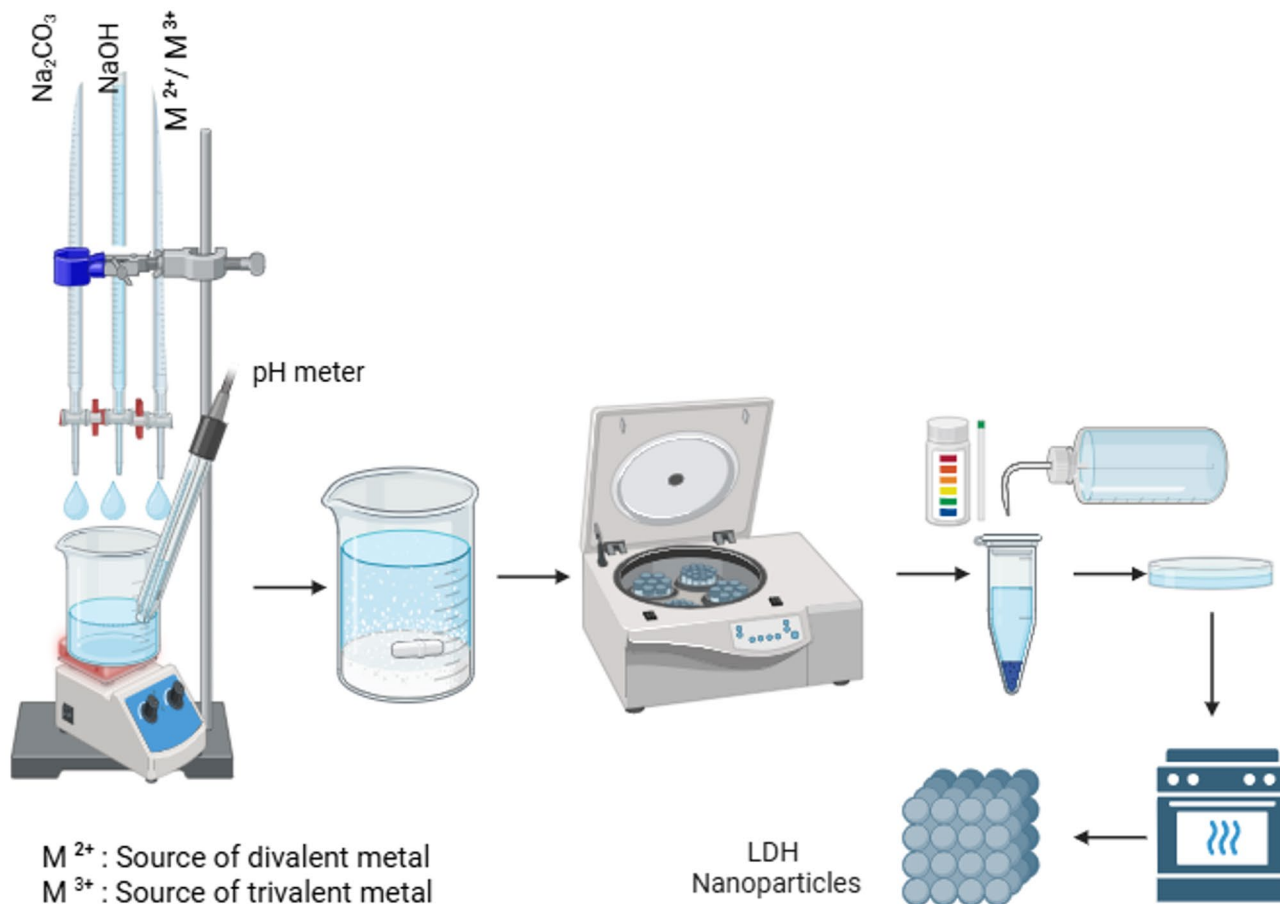
Fig. 1. Schematic of LDH NPs synthesis.

Ni–Fe LDH
This synthesis was the same as the previous step, with the only difference that the molar ratio of trivalent metal to divalent metal was 3:1.

Mn-impregnated Zn–Al LDH
This synthesis was also the same as the previous step, which is finally soaked in magnesium solution.

Purolite A-400 ion exchange resin
Purolite A-400 ion exchange resin was used to investigate its potential for nitrate removal. Purolite A-400 anionic resin is usually used to remove anions from water. It is a strong anionic resin called A-400 that trades chloride ions in a cycle. This means it has all its ions in water, meaning that it can take on all the anions in water and replace them with chloride ions. A sodium chloride salt solution was used to bring this kind of material back to life. The chloride ions in water are replaced with the anions on the resin's surface, which makes the resin less dense. This material is usually used to get rid of nitrates, colors derived from anions, anions that are bad for the environment, like nitrite and fluoride, and anions that make water less useful for industry. The ion-exchange resin was activated and then put into an adsorption column with a certain concentration of nitrate.

Membrane fabrication
Preparation of polysulfone UF membranes with Mn-impregnated Zn–Al LDH NPs
Specifications of the UF membranes are in Table 1. Initially, the Mn-impregnated Zn–Al LDH Nps were dispersed in NMP solvent using an ultrasonic device (Bandelin) at 80 W in 3 intervals of 20 min. Then, polymer and additive were added, and the solution was placed on a stirrer at 60 °C for 24 h to obtain a homogeneous solution. Then, the homogeneous solution was allowed to settle for 1 day for de-bubbling. After that, the polymer solution was cast into a 200 μm thick film on a glass for the phase inversion method using water as anti-solvent at 25 °C. The synthesized UF support membranes were then stored in deionized water for testing.

Preparation of TFC-NF membranes
TFC-NF membranes were formed using the UF support mixed matrix membranes via interfacial polymerization (IP) using two monomers, PIP and TMC, as shown in Fig. 2 and listed in Table 1. For this purpose, the UF membranes containing different concentrations of LDH were first placed in 1% PIP (W/V%) solution for 5 min.

TFC-NF membrane	UF membrane as support layer				Thin layer	
	PSF (wt%)	NMP (wt%)	PVP (wt%)	NPs (wt%)	PIP (W/V%)	TMC (W/V%)
M-LDH-0	15	84	1	0	1	0.1
	UF-LDH-0					
M-LDH-0.25	15	84	1	0.25	1	0.1
	UF-LDH-0.25					
M-LDH-0.5	15	84	1	0.5	1	0.1
	UF-LDH-0.5					
M-LDH-0.75	15	84	1	0.75	1	0.1
	UF-LDH-0.75					
M-LDH-1	15	84	1	1	1	0.1
	UF-LDH-1					

Table 1. Composition of the fabricated UF support membranes and the TFC NF membranes. Membrane-LDH- percentage of Mn-impregnated Zn–Al LDH NPs.
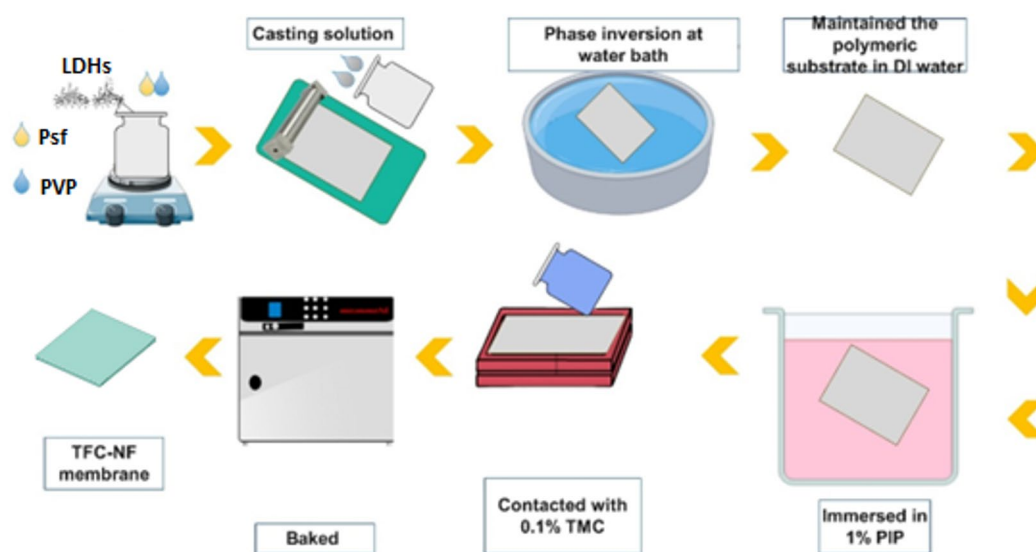
Fig. 2. Synthesis steps of the TFC-NF membranes.

Then, the membranes were exposed to 0.1% TMC (W/V%) for 1 min. Then, the membranes were placed in an oven at 80 °C for 15 min. The membranes were finally placed in distilled water for further investigations.

Preparation of layer-by-layer assembly TFC-NF membranes (TFC-LBL)
In this method, the same TFC membrane without any LDH (M-LDH-0), as before used in the last step, was used to re-layer by the LBL assembly method and modify its surface charge. PDDA (cationic polyelectrolyte) and PSS (anionic polyelectrolyte) materials were utilized for the LBL assembly[37]. The surface charge of the TFC membrane is negative, so with the addition of polycations, it was expected that a positive half-layer to be created on the membrane surface (TFC-0.5), then a half-layer of polyanions was placed on it (TFC-1) and the layering with polycations was repeated as shown in Fig. 3. Finally, a thin layer of GA was applied, as their values are listed in Table 2.

Measurement and characterization techniques
Nanoparticles
X-ray diffraction is a method used to study the structural properties of crystalline materials, including LDH NPs. XRD analysis of LDH samples is expected to confirm their crystalline and phase, as well as the structural configuration of LDH sheets. XRD analysis was done by the Bourevestnik DRON-8 device.

To investigate the chemical structure of LDH samples, Fourier-transform infrared spectroscopy (FTIR Spectrometer - Spectrum 100 (PerkinElmer USA) was used. It is expected to study the NPs' functional groups.

To measure the specific surface area of LDH samples, Brunauer-Emmett-Teller (BET) analysis was used. For this purpose, the synthesized NPs were first heated at temperature of 250 °C so that they became free of moisture
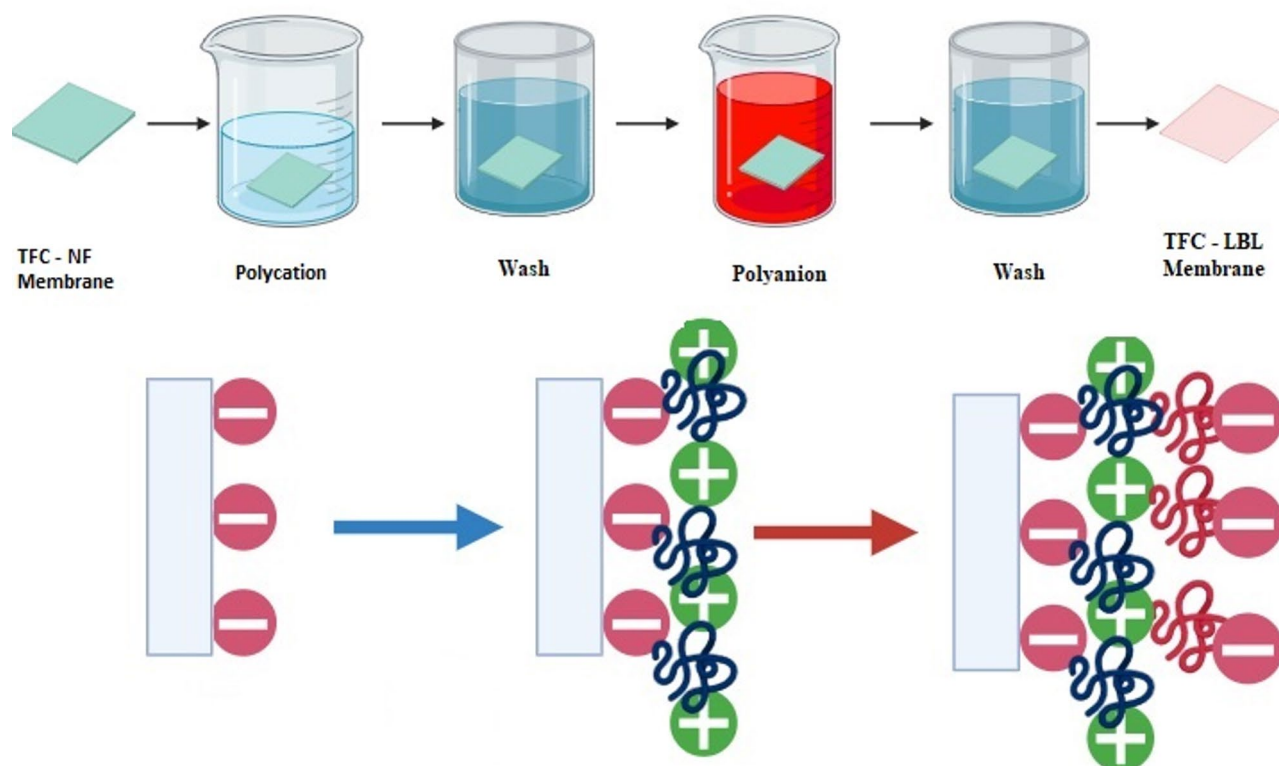
Fig. 3. The steps of layer formation by the LBL assembly method.

	Polycation concentration (M)	Exposure time in polyanion (min)	Polyanion concentration (M)	Exposure time in polyanion (min)	NaCl concentration (M)	The number of layers	GA%	Temperature (°C) and duration of exposure in the oven (h)
TFC-0	0.1	30	0.1	30	0.5	0	0.1	80, 4
TFC-0.5	0.1	30	0.1	30	0.5	0.5	0.1	80, 4
TFC-1	0.1	30	0.1	30	0.5	1	0.1	80, 4
TFC-1.5	0.1	30	0.1	30	0.5	1.5	0.1	80, 4

Table 2. The conditions and concentrations of the LBL assembly method. TFC, The number of layers.

and impurities, and the surface of NPs was activated. Then, BET analysis was performed using the BELSORP-MiniX device in nitrogen gas environment.

The NPs' structure was also observed by field emission scanning electron microscopy (FESEM) analysis using a MIRA3 TESCAN instrument.

The zeta potential of materials is a significant characteristic that illustrates their several water purification's abilities. This metric quantifies the charge associated with repulsion or attraction between particles in solution, a fundamental factor influencing stability of suspended solids, and describes the mechanisms behind dispersion or aggregation. The device used was the ZETA check model, manufactured by Particlemetrix, Germany, and the Czech Republic.

The synthesized NPs were evaluated for their ability to adsorb and remove nitrate ions. To do this, 1 g of NPs was added to nitrate solutions containing 10, 20, 40, 60, 80, and 100 mg/L, and the solution containing NPs was then put on a magnetic stirrer. At certain times, a certain amount of the solution was taken out and accelerated in a centrifuge. The above solution was centrifuged, and the supernatant was thrown away. Nitrate content was measured in ultraviolet-visible (UV-vis, Shimadzu Model-160 A) absorbance of various nitrate solutions at wavelengths of 220 nm and 275 nm[30,35,38].

Then, the subscale relationship was applied to measure the removal rate (R) of nitrate ions as calculated by Eq. (1).

$$R(\%) = \frac{C_0 - C_e}{C_0} \times 100 \tag{1}$$

where C_0 is the initial nitrate concentration and C_e is the equilibrium nitrate concentration in terms of mg/L.

Membranes
FESEM imaging was performed with a Field Emission Scanning Electron Microscope (MIRA3 model made by TESCAN company) to investigate surface morphological changes of the membranes. The membrane samples were fractured using liquid nitrogen and subsequently coated with gold NPs using sputter deposition. FESEM imaging was conducted at an acceleration voltage of 10 kilovolts (kV).

Nanofiltration performance evaluation   The filtering performance of NF membranes was evaluated using a laboratory-scale cross-flow flat membrane module (Fig. 4). PWF was measured at 6 bar after compaction. The feed temperature in the cross-flow cell was kept constant at 25 ± 0.5 °C. The initial evaluation of filtration was conducted using a single-component nitrate salt. However, for desalination, various types of salts were investigated. PWF (J) and nitrate (salt) rejection (R) of the developed membranes were determined by applying Eqs. (2) and (3):

$$J = \frac{V}{A \times t} \tag{2}$$

$$R(\%) = \left(1 - \frac{C_p}{C_f}\right) \times 100 \tag{3}$$

where V(L) is volume of the collected permeate during time interval t as the permeation time (h), A(m^2) is the effective membrane area, and C_p and C_f are concentrations of nitrate (salt) in the permeate and feed solutions, respectively. The nitrate concentrations were measured with a UV-spectrophotometer (UV–Vis, Shimadzu Model-160 A), and salt concentrations were measured using a conductometer (HANNA HI 2300).

Results and discussion
Characterization of NPs
The XRD of Ni–Fe–CO$_3$ LDH, as shown in Fig. 5, exhibits distinct diffraction peaks at 2θ values of about 11.68°, 23.27°, 34.99°, 36.76°, 45.87°, 61.5°, and 65.31°. The peaks could be similar to the 003, 006, 009, 012, 015, 110, and 113 diffraction peaks (JCPDS Pattern 22-0700)[39], respectively. The peaks (003), (006), and (009) can be attributed to the lamellar substance. The diffraction peak at around 61.5° corresponds to the carbonate anions. Indeed, the majority of these peaks display straight and symmetrical properties, hence demonstrating the significant purity of Ni–Fe–CO$_3$ LDH[40].

The XRD patterns of the Mg–Al-uncalcined and Mg–Al-calcined LDHs NPs are presented in Fig. 6. The primary reflections observed at (003), (006), (009), (110), (113), (015), and (018) are consistent with those reported in Cardinale's study[41], indicative of the characteristic diffraction pattern of layered structures. The characteristic peaks of the Ni–Fe LDH NPs exhibited higher intensities compared to those of Mg–Al LDH NPs, which could be attributed to the lower crystallinity of the Mg–Al LDH NPs[36]. It was also observed that during the calcination process, the Mg–Al LDH structure moves towards the amorphous region.
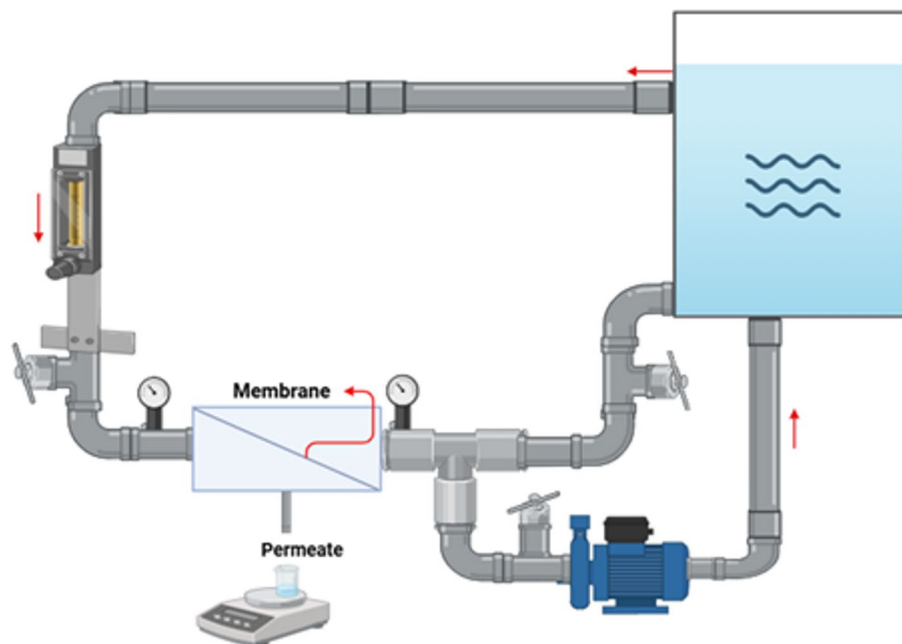

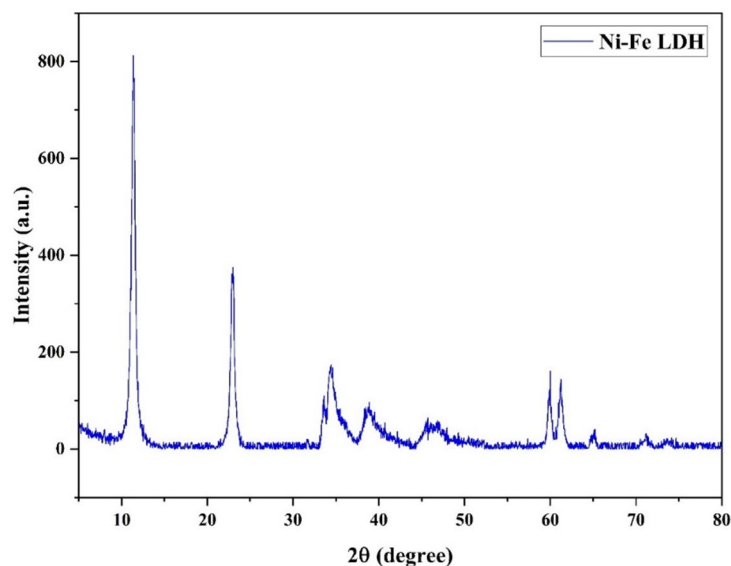**Fig. 4**. General schematic of the filtration process.

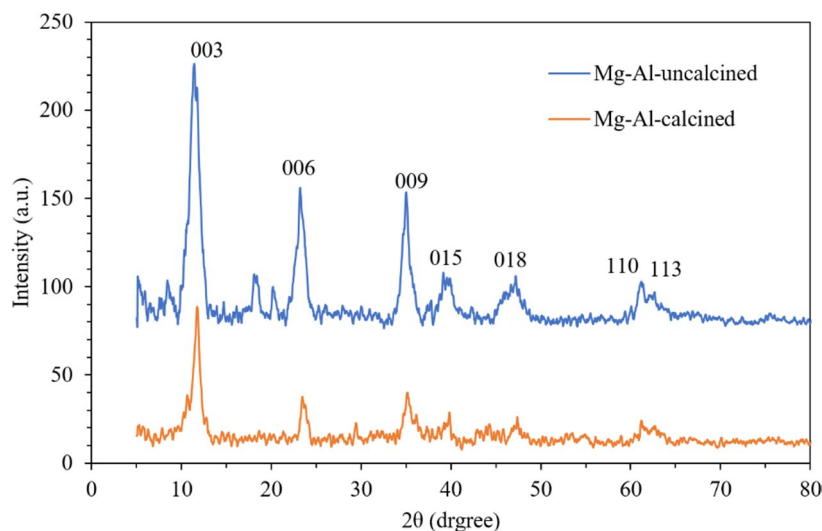**Fig. 5**. XRD patterns of Ni–Fe–CO$_3$ LDH.

Fig. 6. XRD patterns of the Mg–Al-uncalcined and Mg–Al-calcined LDH NPs.

FTIR spectroscopy was employed to analyze the functional groups in Ni–Fe–CO$_3$ LDH NPs (Fig. 7). The band at 3434 cm^{-1} signifies the stretching vibration of the hydroxyl group, the band at 1640 cm^{-1} denotes the bending vibration of water, and the carbonate vibration is observed at 1360 cm^{-1}. Three peaks are seen in the range of 400–700 cm^{-1}, associated with M-O bonds (where M represents Fe^{3+} and Ni^{2+}) in the LDH samples. The FTIR spectrum of the produced sample often aligns with spectra observed in related sources[42].

Additionally, BET analysis was used to describe the surface features of the Ni–Fe–CO$_3$ LDH NPs. The obtained BET results showed that the surface area and total pore volume of the LDH NPs are 82.401 m^2 g^{-1} and 0.5112 cm^3 g^{-1}, respectively. The BET study showed that most of the pores are between 5 and 50 nm in size, which means they are mesopores. The curve of the absorption isotherm can be applied to figure out details about the surface. Table 3 shows a summary of the data about the surface features of Ni–Fe–CO$_3$ LDH NPs.

Surface FESEM images of the Ni–Fe–CO$_3$ LDH NPs are presented in Fig. 8A,B. Specific morphologies are ascribed to the presence of Ni^{2+} ions, which reduces the surface energy differential between polar and nonpolar planes. The depiction of synthesized Ni–Fe–CO$_3$ LDH NPs displays agglomerated grains that form many cavities, therefore enhancing adsorption of anionic species. The image illustrates samples in Fig. 8C,D of Mg–Al–CO$_3$ LDH NPs at standard conditions, exhibiting tiny and diverse sizes. The findings from the isothermal technique of N$_2$ absorption, along with previous studies, consistently indicate the presence of plate-like particles featuring slit pores. The structure seems more porous and exhibits a blend of coral shape with substantial layers. On the
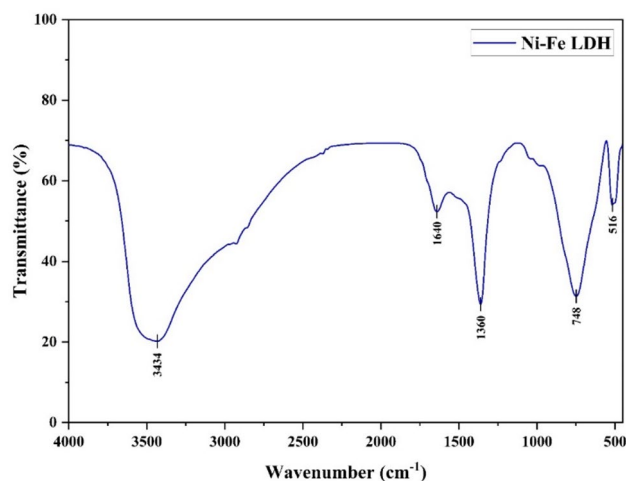
Fig. 7. FTIR spectra of the Ni–Fe–CO$_3$ LDH.

Nanoparticles	a$_{s, BET,}$ m^2 g^{-1}	Total pore volume, cm^3 g^{-1}	Average pore diameter, nm
Ni–Fe–CO$_3$ LDH	82.401	0.5115	24.83

Table 3. BET characterization of the Ni–Fe–CO3 LDH NPs.

other hand, the FESEM approach reveals no changes in the morphology of the solid materials produced with and without calcination, as seen in Fig. 8E,F.

To determine the charge of NPs, their zeta potential was measured and illustrated in Table 4. The measured results indicated average zeta potentials of + 18.5 mV for Mg–Al–CO$_3$ and + 28.2 mV for Ni–Fe–CO$_3$ LDH NPs at pH = 7 which were in agreement with the results obtained by other researchers[43]. According to the results, it is clear that the Ni–Fe–CO$_3$ LDH NPs have higher ability than the Mg–Al–CO$_3$ LDH NPs for nitrate removal. The positive zeta potential of the LDH structures is primarily attributed to the associated positive charge and the electric double layer on the LDH surfaces. While the interior charges of LDH NPs are entirely neutralized by interlayer anions, the surface structural charges remain insufficiently counterbalanced by the adsorbed surface anions, as these anions may separate from the electric double layer on the LDH surfaces, resulting in net positive surface charge on the LDH NPs.

In the nitrate adsorption process, the Ni–Fe LDH NPs showed the highest adsorption rate. As can be seen in Table 4, at pH = 7, the Ni–Fe LDH NPs exhibit the highest zeta potential compared to the Mg–Al LDH and Mn-impregnated Zn–Al LDH NPs. The greater electrostatic interaction between the negatively charged nitrate ions and the positively charged surface of Ni–Fe LDH NPs could be the reason for the higher nitrate adsorption rate. Also, zeta potential of the Ni–Fe LDH NPs was measured in the pH range of 5–9. As can be seen in Fig. 9, the adsorption rate in acidic pH also shows better results due to the electrostatic interactions.

Nitrate removal behavior of the LDH NPs and ion exchange resin was investigated as shown in Fig. 10. As observed, by adding 1 g/L of the NPs in solutions with different concentrations of nitrate, it was found that the NPs could remove nitrate by 6, 7, 14, and 7% by Mg–Al uncalcined LDH, Mg–Al calcined LDH, Ni–Fe LDH, and Mn-impregnated Zn–Al LDH. respectively. However, ion exchange resin was capable of removing 98% of nitrate. Considering the selection of 5 different nitrate concentrations, LDH NPs at concentrations of 100, 80, 60, and 40 mg/L were unable to remove nitrate, and the percentage of nitrate removal was practically negligible. For this reason, the nitrate solution with concentration of 20 mg/L was considered and used as a basis for the experiments in which the removal percentage was measurable.

The highest nitrate adsorption was obtained for the Ni–Fe LDH NPs. Accordingly, EDS analysis was performed for the Ni–Fe LDH NPs before and after the nitrate adsorption process. As seen in Fig. 11, the values of oxygen and nitrogen content increase slightly after the adsorption process. According to this phenomenon, the mechanism of ion exchange and adsorption can be justified in the nitrate removal[44].

Also, according to the published reports[45–48], calcination might increase the amount of nitrate adsorption, so the effect of calcination on Mg-Al LDH was investigated at temperature of 500 °C for 8 h. However, as it turns out, the difference was only 1%. It should be mentioned that, as contradictory reported by Halajnia et al., calcination might not significantly affect the rate of nitrate adsorption[36].

According to the results obtained in this experiment, the effects of various factors on the nitrate adsorption process, such as pH, NPs dose, temperature, and contact time, were investigated. However, the nitrate removal results were still low, and no significant improvement was observed.

Due to the low adsorption of nitrate, the two-step adsorption process was also investigated as reported[49], and the initial nitrate solution in which the adsorption took place was poured again with the same dose of new
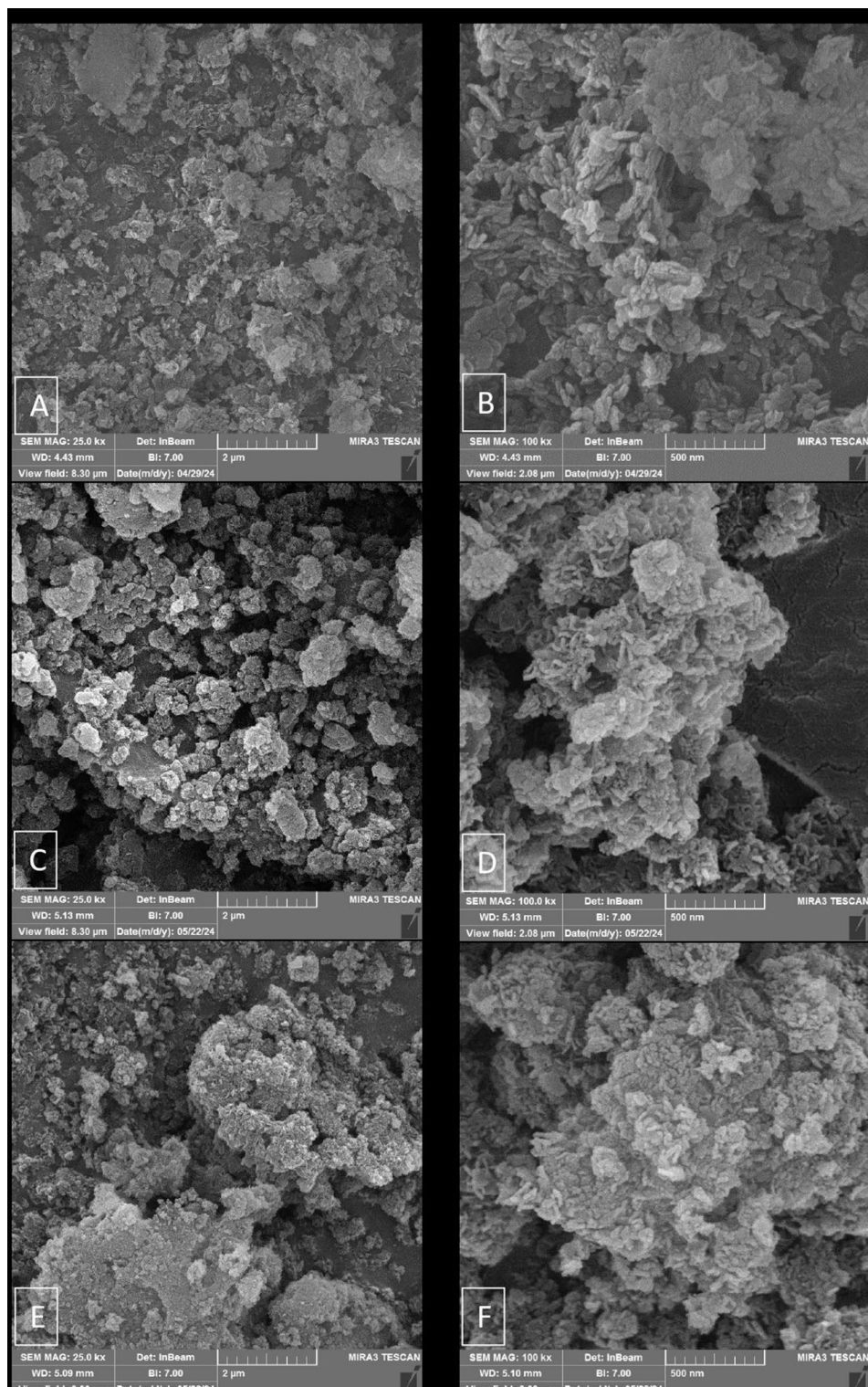
Fig. 8. Surface FESEM images of the (**A,B**) Ni–Fe; (**C,D**) Mg–Al-uncalcined and (**E,F**) Mg–Al-calcined LDH NPs.

adsorbent. The results are seen in Fig. 12. As can be seen, the percentage of nitrate removal is still low and the results are the same as those of the single step adsorption.

Characterization of membranes

FESEM images of the fabricated neat and TFC-NF membranes are shown in Fig. 13. The images show both cross-sectional (A) and top surface (C) view of the fabricated TFC-NF membrane, containing Mn-impregnated Zn–Al

NPs type	Measured value (mV)	pH
Mg–Al LDH	+ 18.5	7.0
Ni–Fe LDH	+ 55.5	5.0
Ni–Fe LDH	+ 28.2	7.0
Ni–Fe LDH	− 29.9	9.0
Mn-impregnated Zn–Al LDH	− 2.5	5.0
Mn-impregnated Zn–Al LDH	− 3.8	9.0

Table 4. Zeta potential of the NPs.
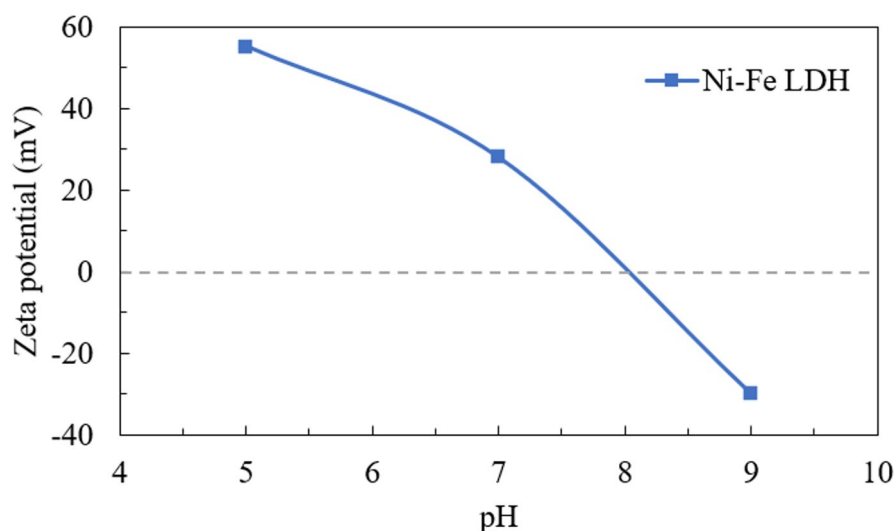
Fig. 9. Zeta potential of the Ni–Fe LDH NPs in the pH range of 5–9.

LDH NPs. Also, cross-section (B) and top surface (D) images of UF-LDH-0 as the neat membrane without NPs are presented. The surface images indicate a significant shift in morphology, where more micropores can be seen in the NPs containing membrane compared to the neat membrane. Importantly, no defect on the membrane surface is found after adding NPs to the casting solution. The growth of finger-like protrusions downward from the thin surface layer is obvious. Considering that LDH is a hydrophilic material, the presence of hydrophilic LDH enhances thermodynamic instability in the polymer solution and eventually leads to faster mixing between solvent and non-solvent in the coagulation bath. Rapid mixing causes the membrane cross-sectional area to contain additional pores. As one can see, the neat membrane structure is much thicker than the NPs loaded membrane and has more holes that can foam up. Also, finger-like holes are only present in the upper part of this membrane, and they are not observed in its bottom part. When Mn-impregnated Zn–Al LDH NPs are added to the support of the UF polymer matrix, the membrane porosity goes up. Bigger finger-like holes are formed in the membrane structure, and they go all the way to the bottom. As mentioned, this is because Mn-impregnated Zn–Al LDH NPs are hydrophilic, and accelerate the exchange rate of solvent and non-solvent during the phase inversion process. Having hydrophilic NPs in the polymer matrix increases the flow of water into the polymer layer and makes it easier for membranes with bigger pores to form[50].

Additionally, EDX mapping was conducted to analyze the elemental distribution within the Mn-impregnated Zn–Al LDH NPs-incorporated membranes (Fig. 14). The results indicated that all elements are uniformly distributed throughout the M-LDH-0.25 membrane.

The AFM analysis results for the UF-LDH-0, UF-LDH-0.25, M-LDH-0.25 and Mn-impregnated Zn–Al LDH NPs are revealed in Fig. 15. The UF-LDH-0 membrane (A), shows the lowest surface roughness, and after adding the Mn-impregnated Zn–Al LDH NPs (D), which have the highest roughness among the images, surface roughness of the UF-LDH-0.25 membrane (B), increases. As illustrated in Fig. 15, the M-LDH-0.25 membrane (C), exhibits reduced surface roughness compared to the UF-LDH-0.25 membrane, owing to the successful completion of the IP process[51].

The M-LDH-0 membrane exhibits relatively low water permeability of 3.8 LMH bar^{-1}. When being doped with Mn-impregnated Zn–Al LDH NPs possessing a negatively charged surface between − 2.5 and − 3.8 mV in the pH range of 5 to 9 (Table 4), water permeability is remarkably raised to 7.5 LMH bar^{-1} at the concentration of 0.75 wt%. This might benefit from the synergetic effects of (1) additional water transport channels from the support UF membrane by adding Mn-impregnated Zn–Al LDH NPs, (2) an increased water filtration area from the higher surface roughness, and (3) the improved surface hydrophilicity. A further increase in the LDH loading results in reduced PWF due to the formation of stacked layers or agglomerated LDH NPs, which reduce
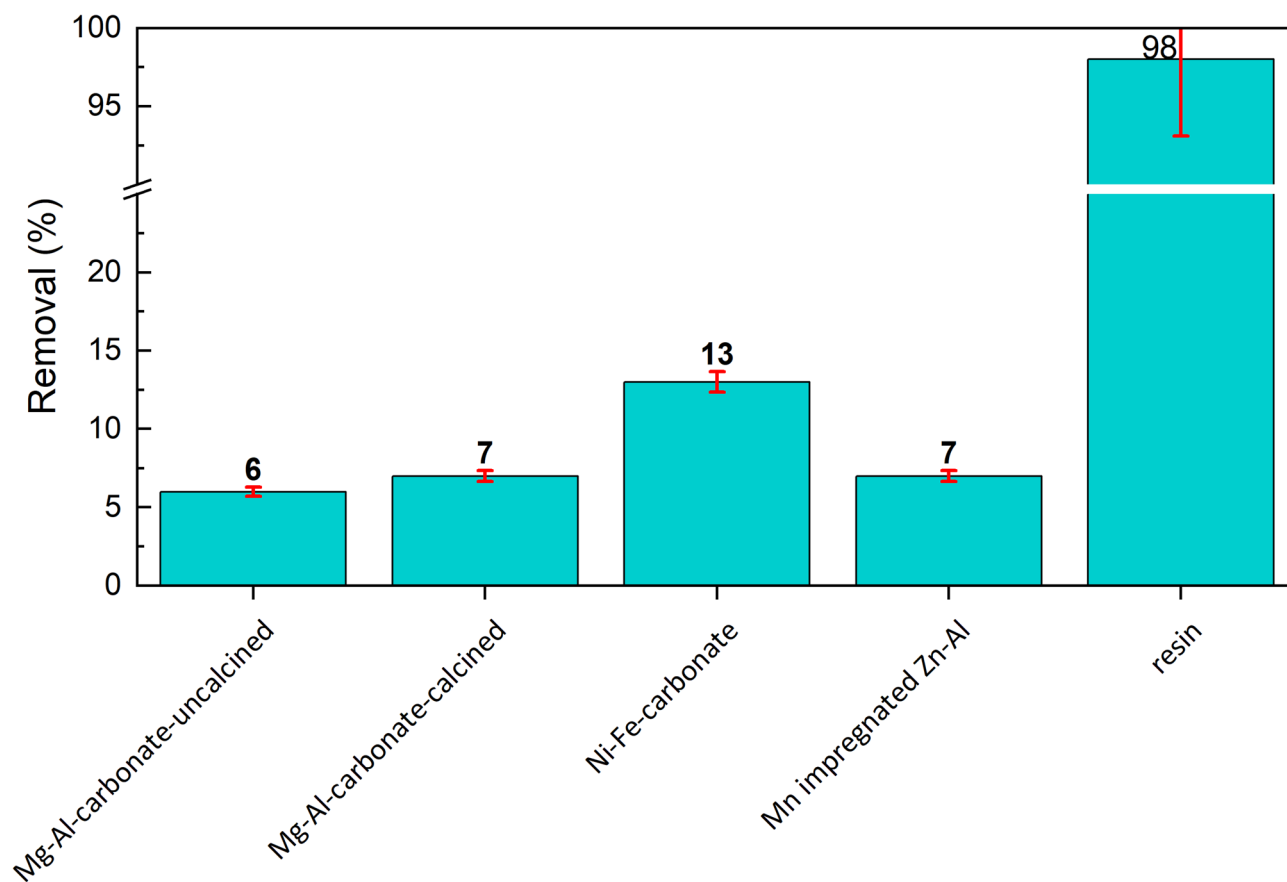
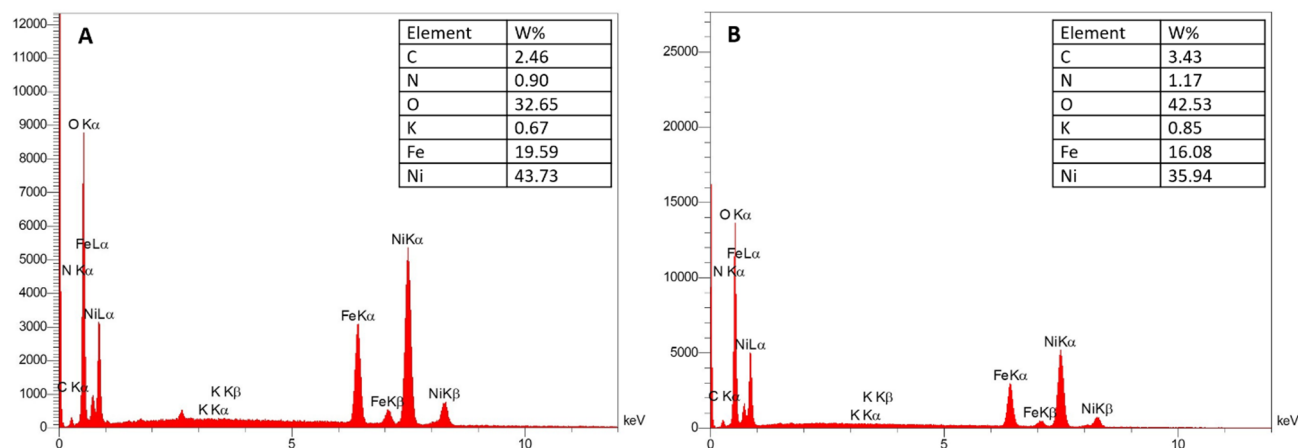**Fig. 10**. Nitrate removal behavior of the LDH NPs and commercial resin in the nitrate solution (20 mg/L).

Fig. 11. EDS results of the Ni–Fe–CO$_3$ LDH NPs before and after NO$_3^-$ adsorption.

the pathways for water transport[52–54]. Figure 16 represents rejection behavior of the TFC-NF membranes for different types of inorganic salts (MgSO$_4$, MgCl$_2$, Na$_2$SO$_4$, KNO$_3$, and NaCl). As seen, the descending order of salt rejection follows this order Na$_2$SO$_4$ > MgSO$_4$ > MgCl$_2$ > NaCl > KNO$_3$. For NF membranes, separation mechanisms are highly influenced via the combined effects of size exclusion (steric hindrance) and Donnan exclusion[55].

As all the membranes possessed negative surface charge (and the membranes' surface zeta potential values were negative due to the concentrations of PIP and TMC used[56], higher rejections of divalent anions rather than monovalent anions were observed due to the stronger electrostatic repulsion of higher-valent anions. Thus, higher rejection was obtained for Na$_2$SO$_4$ and MgSO$_4$ than MgCl$_2$, NaCl, and KNO$_3$[57]. Furthermore, the lower
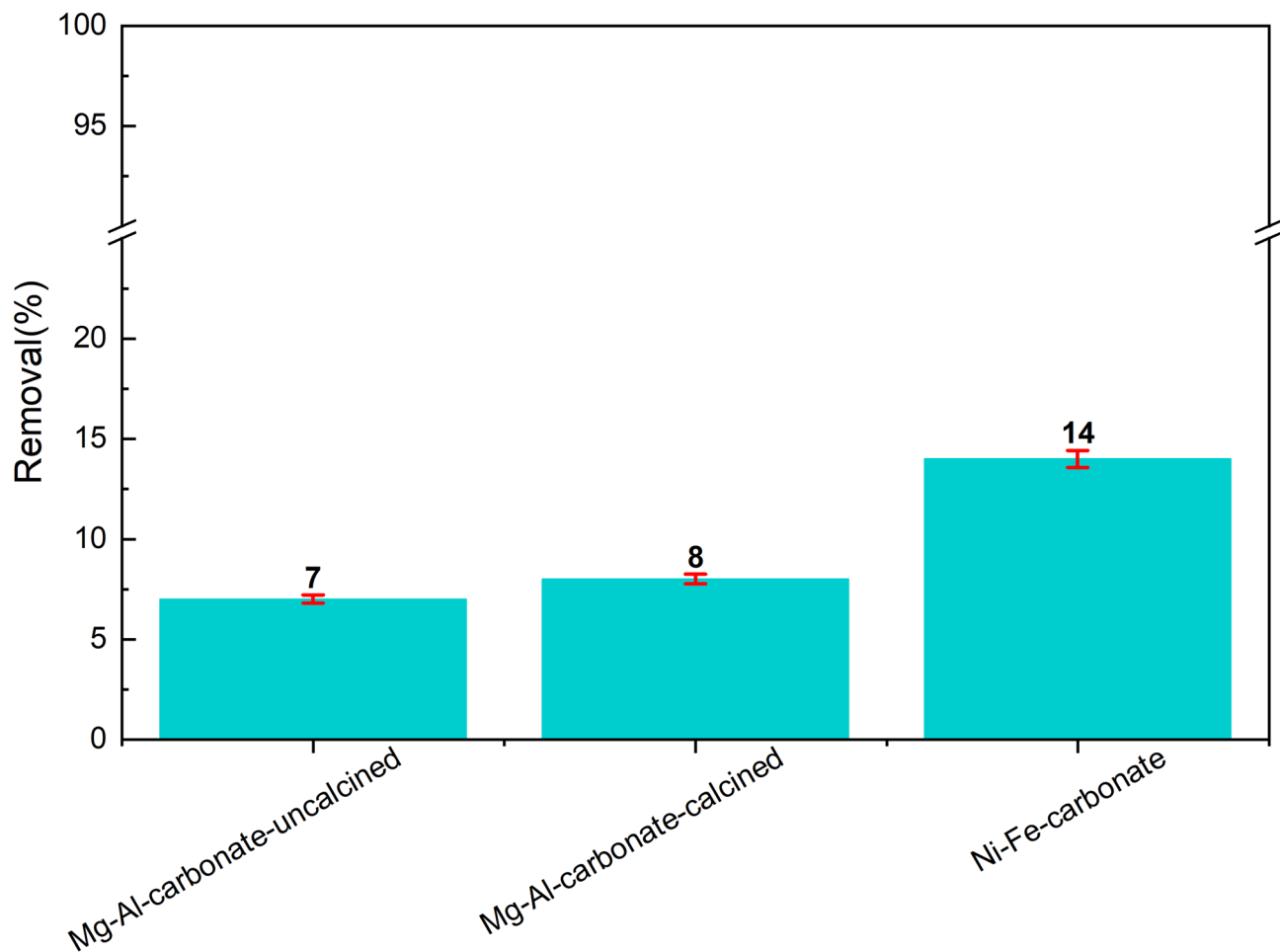
Fig. 12. Nitrate removal behavior of the LDH NPs based on the two-step adsorption method.

rejection of NaCl compared to $MgCl_2$ was also attributed to the higher diffusivity of Na^+ ions than Mg^{2+} ions[53]. The ionic radius, hydrated radius, and diffusion coefficient of ions are given in Table 5.

Among the synthesized membranes, the M-LDH-0.25 membrane performed better nitrate rejection (43%) compared to the other membranes. Hydration of nitrate ions in water can occur through hydrogen bonding between oxygen atom of the nitrate and hydrogen atom of water molecules. However, nitrate ions can easily undergo dehydration near (or in) the membrane pores because hydrogen bonds are weak, so rapid and frequent exchange of water molecules in the solubility shells of nitrate ions can occur. Due to the weak hydration effect of nitrate ions, its rejection was reported to be low[58].

Characterization of TFC-LBL NF membranes

According to Fig. 17, as seen, the TFC-0 (neat TFC-NF) membrane exhibits water permeability as 10.3 LMH bar^{-1}. Compared to the neat TFC-NF membrane, the LBL assembly membranes exhibit reduced water permeability, with lower water permeability at higher bilayer number. This can be attributed to the higher resistance to water permeation with the thicker polyelectrolyte multilayer[37].

The membrane with positive surface charge (TFC-0.5) exhibits higher rejection of $MgSO_4$ than Na_2SO_4. However, strong electrostatic attraction of the membrane surface negative charge (TFC-0 and TFC-1) to divalent Mg^{2+} ions weakens the effectiveness of Donnan exclusion, so rejection of $MgSO_4$ is slightly lower than Na_2SO_4[59].

As seen in Fig. 17 for the TFC-LBL NF membranes, the nitrate removal rate increases slightly with increasing the number of positively charged layers. This could be due to the adsorption of nitrate ion with negative charge into the positively charged layers of PDDA, a cationic polyelectrolyte with quaternary ammonium groups via electrostatic attraction mechanism. The adsorption of nitrate by the PDDA layer was effectively represented by the Freundlich isotherm, and its uptake kinetics was closely followed the pseudo-second-order model[60].

In the TFC-1.5 membrane, due to the thicker polyelectrolyte multilayer, diffusion of ions reduces, and as a result, ions rejection improves. Also, the membrane pore size becomes smaller and this improves ions rejection. Also, reducing the membrane pore size increases nitrate rejection through the size exclusion (steric hindrance) mechanism, and it is argued that the size of nanopores has greater effect than the surface charge on nitrate rejection.
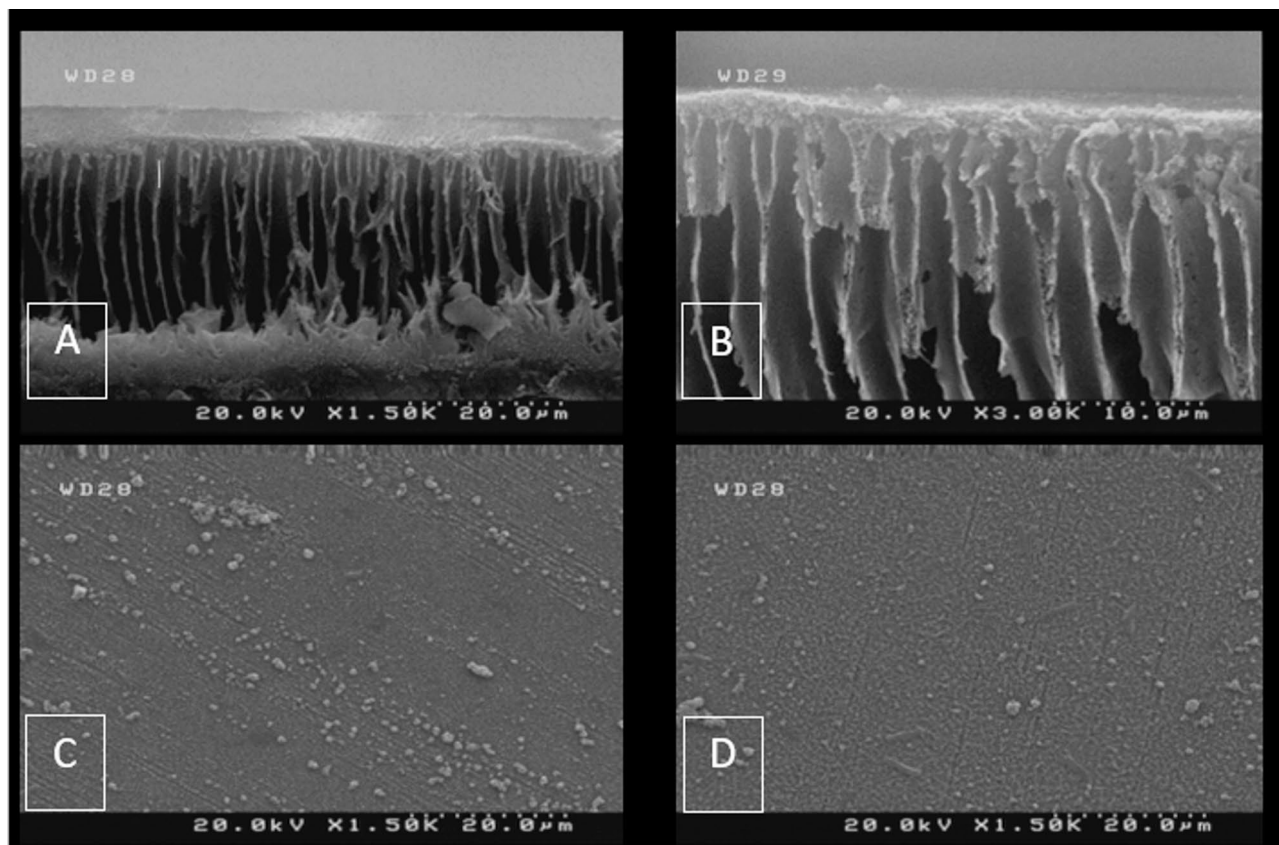
Fig. 13. FESEM images (**A**) (cross section), and (**C**) (top surface) for the membrane with Mn-impregnated Zn–AL LDH NPs; and (**B**) (cross section), and (**D**) (top surface) for M-LDH-0 as the neat membrane.
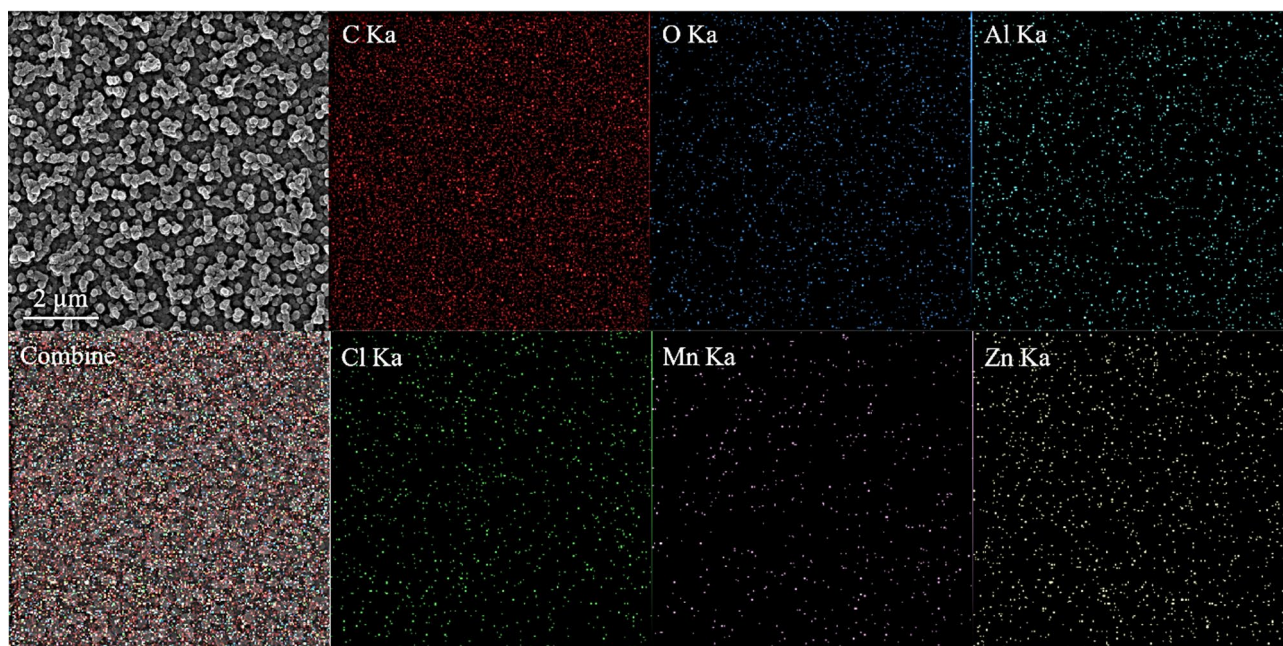

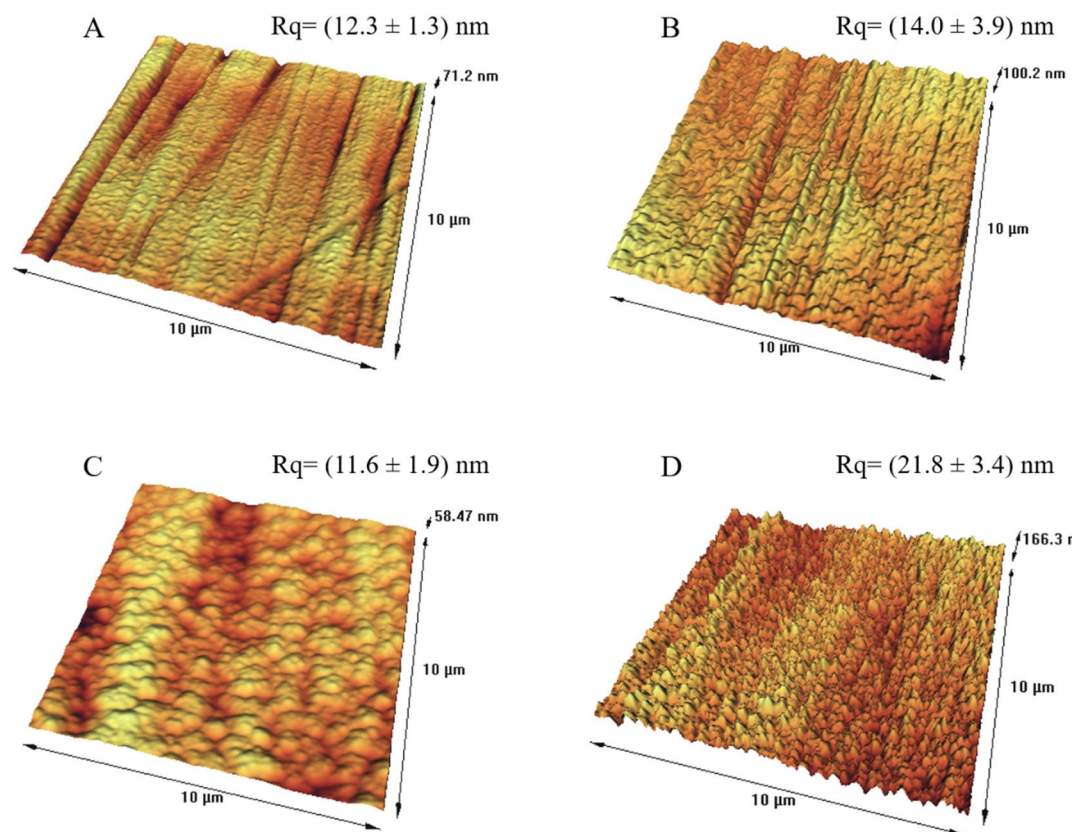**Fig. 14**. EDX mapping of the M-LDH-0.25 membrane.

Fig. 15. AFM images of the (**A**) UF-LDH-0, (**B**) UF-LDH-0.25, (**C**) M-LDH-0.25 and (**D**) Mn-impregnated Zn–Al LDH NPs.

Conclusions

This study focused on nitrate removal from water using NF membranes with support layers containing LDH NPs synthesized by the co-precipitation method, which were used in synthesis of TFC-NF membranes and LBL assembly NF membranes.

Moreover, the results obtained showed that, contrary to previous reports, LDH NPs have limited ability to remove nitrate ions. The Ni-Fe LDH NPs were only able to remove 14% of nitrate ions. The membrane containing 0.25 wt% of the Mn-impregnated Zn-Al LDH NPs exhibited the best performance, achieving PWF of 4.4 LMH bar^{-1} and nitrate rejection of 43% when 50 mg/L KNO$_3$ solution was employed as the feed at 6 bar and 25 ± 1 °C. Despite the disability of LDHs to remove nitrate ions, it was observed that significant level of water permeability could be achieved (97.37%) due to the hydrophilic nature of NPs.
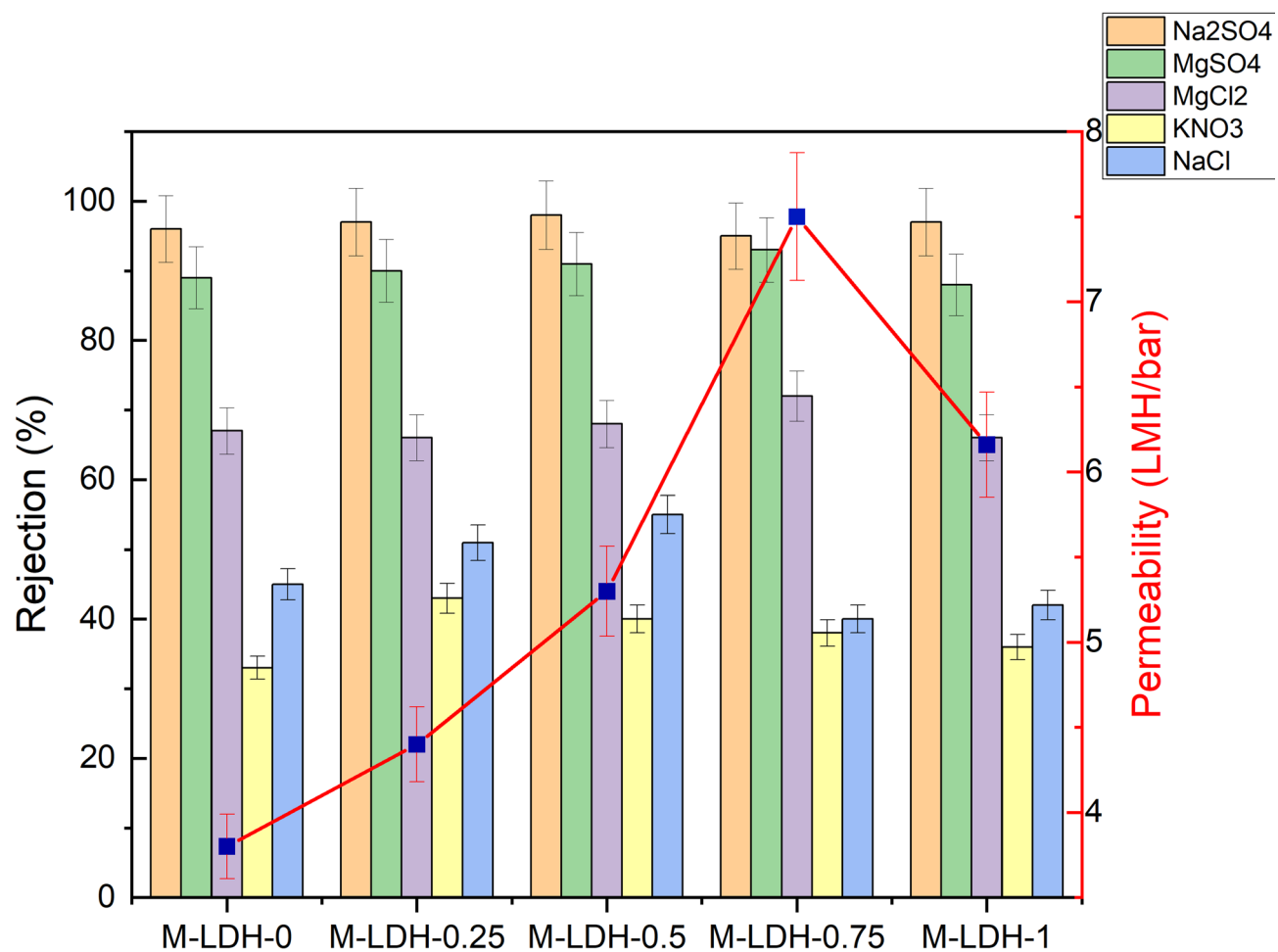
Fig. 16. Nitrate rejection and water permeability of the Mn-impregnated Zn–Al LDH membranes with different NPs concentrations.

Ions	Ionic radius (nm)	Hydrated radius (nm)	Diffusivity coefficient ($\frac{m^2}{s}$)
Na^{+}[53]	0.10	0.36	1.33×10^{-9}
Mg^{2+}[53]	0.07	0.43	0.71×10^{-9}
Cl^{-}[53]	0.18	0.33	2.03×10^{-9}
SO_4^{2-}[53]	0.29	0.38	1.07×10^{-9}
NO_3^{-}[58]	0.18	0.34	–

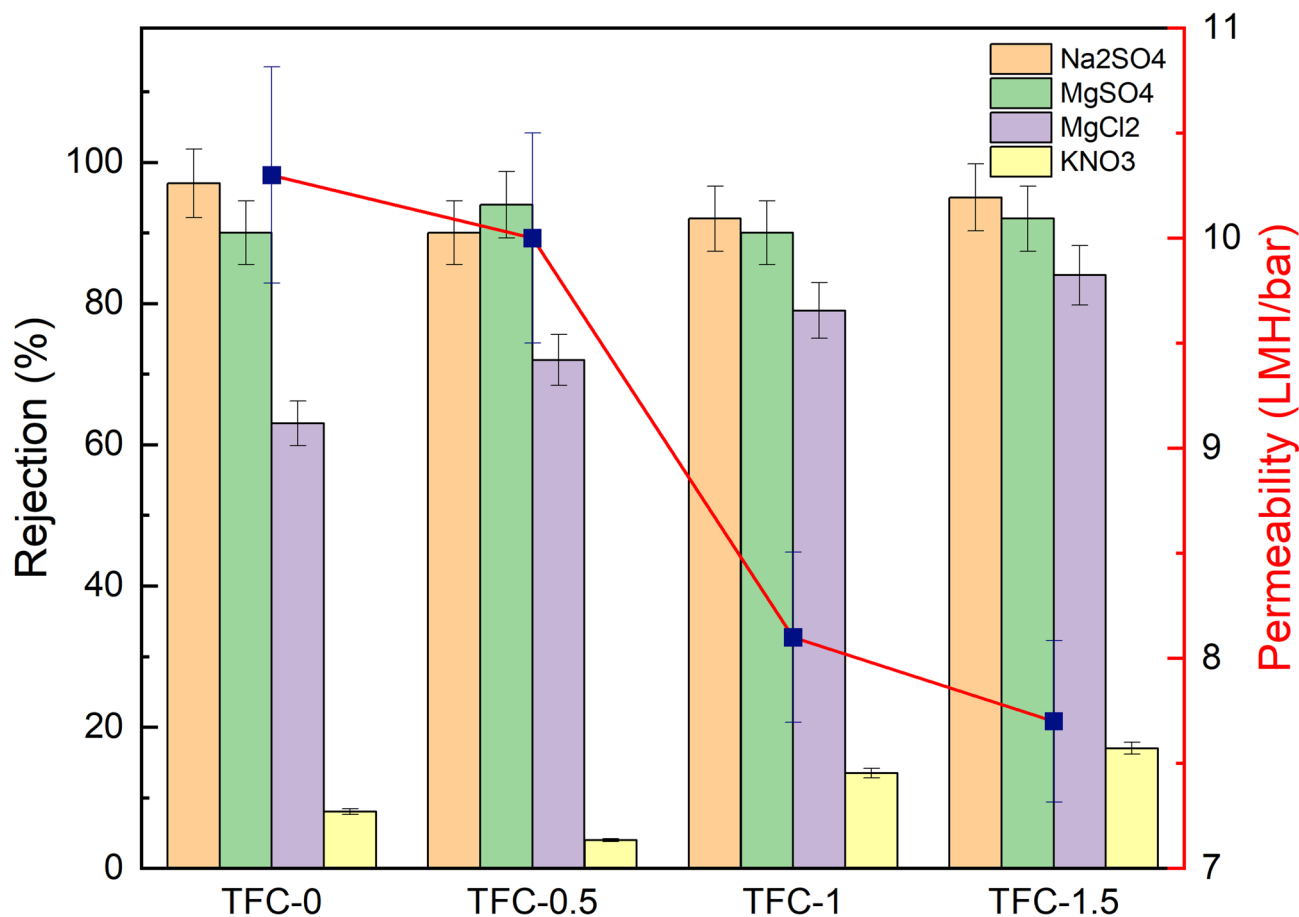**Table 5**. Ion radius, hydrated radius, and diffusion coefficient of ions.

Fig. 17. Nitrate rejection and water permeability of the TFC-LBL membranes with different number of layers.

Data availability
All data generated or analysed during this study are included in this published article.

References
1. He, C. et al. Future global urban water scarcity and potential solutions. *Nat. Commun.* **12**, 4667 (2021).
2. Lin, L., Yang, H. & Xu, X. Effects of water pollution on human health and disease heterogeneity: a review. *Front. Environ. Sci.* **10**, 880246 (2022).
3. Lakhotia, S. R., Mukhopadhyay, M. & Kumari, P. Cerium oxide nanoparticles embedded thin-film nanocomposite nanofiltration membrane for water treatment. *Sci. Rep.* **8**, 4976 (2018).
4. Matei, A. & Racoviteanu, G. Review of the technologies for nitrates removal from water intended for human consumption. In *IOP Conf. Ser. Earth Environ. Sci.*, vol. 664, 12024 (IOP Publishing, 2021).
5. Liu, Y., Zhang, X. & Wang, J. A critical review of various adsorbents for selective removal of nitrate from water: Structure, performance and mechanism. *Chemosphere.* **291**, 132728 (2022).
6. Choudhary, M., Muduli, M. & Ray, S. A comprehensive review on nitrate pollution and its remediation: conventional and recent approaches. *Sustain. Water Resour. Manag.* **8**, 113 (2022).
7. Garcia Torres, E. et al. Consumption of water contaminated by nitrate and its deleterious effects on the human thyroid gland: a review and update. *Int. J. Environ. Health Res.* **32**, 984–1001 (2022).
8. Karwowska, M. & Kononiuk, A. Nitrates/nitrites in food—Risk for nitrosative stress and benefits. *Antioxidants.* **9**, 241 (2020).
9. Singh, S. et al. Nitrates in the environment: A critical review of their distribution, sensing techniques, ecological effects and remediation. *Chemosphere* **287**, 131996 (2022).
10. Touir, J. et al. Nanofiltration and reverse osmosis membrane for nitrate removal: performance study and economic evaluation. *Moroccan J. Chem.* **9**, J–Chem (2021).
11. Alizadeh, M., Noori, R., Omidvar, B., Nohegar, A. & Pistre, S. Human health risk of nitrate in groundwater of Tehran–Karaj plain, Iran. *Sci. Rep.* **14**, 7830 (2024).
12. Rajta, A., Bhatia, R., Setia, H. & Pathania, P. Role of heterotrophic aerobic denitrifying bacteria in nitrate removal from wastewater. *J. Appl. Microbiol.* **128**, 1261–1278 (2020).
13. Pang, Y. & Wang, J. Various electron donors for biological nitrate removal: A review. *Sci. Total Environ.* **794**, 148699 (2021).
14. Liu, X., Huang, M., Bao, S., Tang, W. & Fang, T. Nitrate removal from low carbon-to-nitrogen ratio wastewater by combining iron-based chemical reduction and autotrophic denitrification. *Bioresour. Technol.* **301**, 122731 (2020).
15. Labarca, F. & Bórquez, R. Comparative study of nanofiltration and ion exchange for nitrate reduction in the presence of chloride and iron in groundwater. *Sci. Total Environ.* **723**, 137809 (2020).

16. Fateminia, R., Rowshanzamir, S. & Mehri, F. Synergistically enhanced nitrate removal by capacitive Deionization with activated carbon/PVDF/polyaniline/ZrO2 composite electrode. *Sep. Purif. Technol.* **274**, 119108 (2021).

17. Razvan, A. et al. Nanocomposite membranes prepared from cellulose acetate or polysulfone with Ag0 nanoparticles and Nitron reagent for nitrate ion removal. *Desalin. Water Treat.* **318**, 100400 (2024).

18. Priya, E., Kumar, S., Verma, C., Sarkar, S. & Maji, P. K. A comprehensive review on technological advances of adsorption for removing nitrate and phosphate from waste water. *J. Water Process. Eng.* **49**, 103159 (2022).

19. Bashir, N. et al. Green-synthesized silver nanoparticle-enhanced nanofiltration mixed matrix membranes for high-performance water purification. *Sci. Rep.* **15**, 1001 (2025).

20. Bargeman, G. Recent developments in the preparation of improved nanofiltration membranes for extreme pH conditions. *Sep. Purif. Technol.* **279**, 119725 (2021).

21. Hilal, N., Al-Zoubi, H., Darwish, N. A., Mohamma, A. W. & Arabi, M. A. A comprehensive review of nanofiltration membranes: Treatment, pretreatment, modelling, and atomic force microscopy. *Desalination* **170**, 281–308 (2004).

22. Samavati, Z., Samavati, A., Goh, P. S., Ismail, A. F. & Abdullah, M. S. A comprehensive review of recent advances in nanofiltration membranes for heavy metal removal from wastewater. *Chem. Eng. Res. Des.* **189**, 530–571 (2023).

23. Wu, X. et al. A critical review on polyamide and polyesteramide nanofiltration membranes: emerging monomeric structures and interfacial polymerization strategies. *Desalination* 117379 (2024).

24. Li, S. et al. Recent advances on cellulose-based nanofiltration membranes and their applications in drinking water purification: A review. *J. Clean. Prod.* **333**, 130171 (2022).

25. Hafiz, M., Hawari, A. H., Alfahel, R., Hassan, M. K. & Altaee, A. Comparison of nanofiltration with reverse osmosis in reclaiming tertiary treated municipal wastewater for irrigation purposes. *Membr. (Basel).* **11**, 32 (2021).

26. Mehenktaş, C. & Arar, Ö. Application of membrane processes for nitrate (NO3-) removal. *Curr. Chin. Sci.* **3**, 42–56 (2023).

27. Mahvi, A. H., Malakootian, M., Fatehizadeh, A. & Ehrampoush, M. H. Nitrate removal from aqueous solutions by nanofiltration. *Desalin. Water Treat.* **29**, 326–330 (2011).

28. Ghanbari, N. & Ghafuri, H. Preparation of novel Zn–Al layered double hydroxide composite as adsorbent for removal of organophosphorus insecticides from water. *Sci. Rep.* **13**, 10215 (2023).

29. Yue, R. et al. The role of pH on structure, corrosion behavior and biocompatibility of MgFe layered double hydroxide coating on Mg–Nd–Zn–Zr alloy. *Sci. Rep.* **15**, 1–16 (2025).

30. da Silva, A. F. et al. Mechanistic insights of nitrate removal by MgFe/layered double hydroxides prepared by different synthesis pathways. *Appl. Surf. Sci. Adv.* **18**, 100460 (2023).

31. Sokol, D. et al. Sonication accelerated formation of Mg–Al-phosphate layered double hydroxide via sol–gel prepared mixed metal oxides. *Sci. Rep.* **9**, 10419 (2019).

32. Chu, L. et al. Adsorption of nitrate from interflow by the Mg/Fe calcined layered double hydroxides. *Water Sci. Technol.* **86**, 511–529 (2022).

33. Wang, W., Zhu, Q., Huang, R. & Hu, Y. Adsorption of nitrate in water by CTAB-modified MgFe layered double hydroxide composite Biochar at low temperature: adsorption characteristics and mechanisms. *J. Environ. Chem. Eng.* **11**, 109090 (2023).

34. Jiang, Z. et al. Synergistic effect of LDHs/loofah composites for in-situ remediation of nitrate in contaminated groundwater. *Sep. Purif. Technol.* **336**, 126306 (2024).

35. Cano, L. A., Barrera, D., Villarroel-Rocha, J. & Sapag, K. Influence of the synthesis method of layered double hydroxides on the textural properties and nitrate removal. *Catal. Today.* **422**, 114222 (2023).

36. Halajnia, A., Oustan, S., Najafi, N., Khataee, A. R. & Lakzian, A. The adsorption characteristics of nitrate on Mg–Fe and Mg–Al layered double hydroxides in a simulated soil solution. *Appl. Clay Sci.* **70**, 28–36 (2012).

37. Cheng, W. et al. Selective removal of divalent cations by polyelectrolyte multilayer nanofiltration membrane: role of polyelectrolyte charge, ion size, and ionic strength. *J. Membr. Sci.* **559**, 98–106 (2018).

38. Azadbakht, P., Pourzamani, H., Petroudy, S. R. J. & Bina, B. Removal of nitrate from aqueous solution using nanocrystalline cellulose. *Int. J. Environ. Health Eng.* **5**, 17 (2016).

39. Mokhtar, M., Saleh, T. S. & Basahel, S. N. Mg–Al hydrotalcites as efficient catalysts for aza-Michael addition reaction: A green protocol. *J. Mol. Catal. Chem.* **353**, 122–131 (2012).

40. Ahmed, I. M., Abd-Elhamid, A. I., Aly, A. A., Bräse, S. & Nayl, A. A. Synthesis of Ni–Fe–CO3 layered double hydroxide as effective adsorbent to remove cr (VI) and ARS-dye from aqueous media. *Environ. Technol. Innov.* **31**, 103214 (2023).

41. Cardinale, A. M., Carbone, C., Molinari, S., Salviulo, G. & Ardini, F. MgAl-NO3 LDH: adsorption isotherms and multivariate optimization for cr (VI) removal. *Chem. (Easton).* **5**, 633–645 (2023).

42. Liu, X., Shi, J., Bai, X. & Wu, W. Ultrasound-excited hydrogen radical from NiFe layered double hydroxide for preparation of ultrafine supported Ru nanocatalysts in hydrogen storage of N-ethylcarbazole. *Ultrason. Sonochem.* **81**, 105840 (2021).

43. Zhao, Y., Li, N., Xu, B., Dong, B. & Xia, S. Preparation and characterization of a novel hydrophilic Poly (vinylidene fluoride) filtration membrane incorporated with Zn–Al layered double hydroxides. *J. Ind. Eng. Chem.* **39**, 37–47 (2016).

44. Singha Roy, A., Kesavan Pillai, S. & Ray, S. S. Layered double hydroxides for sustainable agriculture and environment: an overview. *ACS Omega.* **7**, 20428–20440 (2022).

45. Islam, M. & Patel, R. Nitrate sorption by thermally activated Mg/Al chloride hydrotalcite-like compound. *J. Hazard. Mater.* **169**, 524–531 (2009).

46. Zhou, H., Tan, Y., Gao, W., Zhang, Y. & Yang, Y. Selective nitrate removal from aqueous solutions by a hydrotalcite-like absorbent FeMgMn-LDH. *Sci. Rep.* **10**, 16126 (2020).

47. Islam, M. & Patel, R. Synthesis and physicochemical characterization of Zn/Al chloride layered double hydroxide and evaluation of its nitrate removal efficiency. *Desalination* **256**, 120–128 (2010).

48. Ivánová, D., Albert, P. & Kavuličová, J. Nitrate removal from model aqueous solutions and real water by calcined Mg/Al layered double hydroxides. *Appl. Clay Sci.* **152**, 65–72 (2018).

49. Öztürk, N. & Bektaş, T. E. Nitrate removal from aqueous solution by adsorption onto various materials. *J. Hazard. Mater.* **112**, 155–162 (2004).

50. Raicopol, M. D., Andronescu, C., Voicu, S. I., Vasile, E. & Pandele, A. M. Cellulose acetate/layered double hydroxide adsorptive membranes for efficient removal of pharmaceutical environmental contaminants. *Carbohydr. Polym.* **214**, 204–212 (2019).

51. Seah, M. Q. et al. Progress of interfacial polymerization techniques for polyamide thin film (nano) composite membrane fabrication: a comprehensive review. *Polym. (Basel).* **12**, 2817 (2020).

52. Zhao, Q., Zhao, D. L., Feng, F., Chung, T-S & Chen, S. B. Thin-film nanocomposite reverse osmosis membranes incorporated with citrate-modified layered double hydroxides (LDHs) for brackish water desalination and Boron removal. *Desalination* **527**, 115583 (2022).

53. Tajuddin, M. H. et al. Incorporation of layered double hydroxide nanofillers in polyamide nanofiltration membrane for high performance of salts rejections. *J. Taiwan. Inst. Chem. Eng.* **97**, 1–11 (2019).

54. Mutharasi, Y., Zhang, Y., Weber, M., Maletzko, C. & Chung, T-S Novel reverse osmosis membranes incorporated with Co-Al layered double hydroxide (LDH) with enhanced performance for brackish water desalination. *Desalination* **498**, 114740 (2021).

55. Rezania, J., Vatanpour, V., Shockravi, A. & Ehsani, M. Preparation of novel carboxylated thin-film composite polyamide-polyester nanofiltration membranes with enhanced antifouling property and water flux. *React. Funct. Polym.* **131**, 123–133 (2018).

56. Lan, H. et al. Fabrication of high performance nanofiltration membrane by construction of Noria based nanoparticles interlayer. *Sep. Purif. Technol.* **290**, 120781 (2022).

57. Xie, Q. et al. Enhancing the performance of thin-film nanocomposite nanofiltration membranes using MAH-modified GO nanosheets. *RSC Adv.* **7**, 54898–54910 (2017).
58. Popova, A. et al. Evaluating the potential of nanofiltration membranes for removing ammonium, nitrate, and nitrite in drinking water sources. *Water Res.* **244**, 120484 (2023).
59. Zheng, F. & Wang, Y. Removal of antibiotics and antibiotic resistance genes by self-assembled nanofiltration membranes with tailored selectivity. *J. Membr. Sci.* **659**, 120836 (2022).
60. Zhang, H., Huang, W. & Komarneni, S. Polymer-clay nanocomposites for the uptake of hazardous anions. *Nanomaterials* **14**, 467 (2024).

Acknowledgements

Author contributions

H.H.M.S.J.: Methodology, investigation, formal analysis, validation, writing-original draft, visualization. Z.Z.: Methodology, formal analysis, validation, writing-original draft, visualization. T.M.: Conceptualization, resources, writing-review and editing, supervision, project administration, funding acquisition. A.A.: Resources, project administration, funding acquisition.

Declarations

Competing interests

The authors declare no competing interests.

Additional information

Correspondence and requests for materials should be addressed to T.M.

Reprints and permissions information is available at www.nature.com/reprints.

Publisher's note Springer Nature remains neutral with regard to jurisdictional claims in published maps and institutional affiliations.